4.3 TRIDIMENSIONAL IMAGES OF VOLCANIC STRUCTURES AND HIDDEN INTRUSIVE BODIES AS INFERRED FROM THE INTERPRETATION OF GRAVITY AND GEOMAGNETIC MODELS

4.3.1. STARTING MODELS FOR NUMERICAL SIMULATION APPROACH (VERSION 0)

4.3.1.1. Location of the studied area

The Ciomadul volcano, one of the youngest structures of the Neogene-Quaternary volcanism of East Carpathians, has been chosen for the construction of a 3D numerical model. Fig. 4.3.1.1 shows location of this volcano within the Călimani-Gurghiu-Harghita volcanic chain.

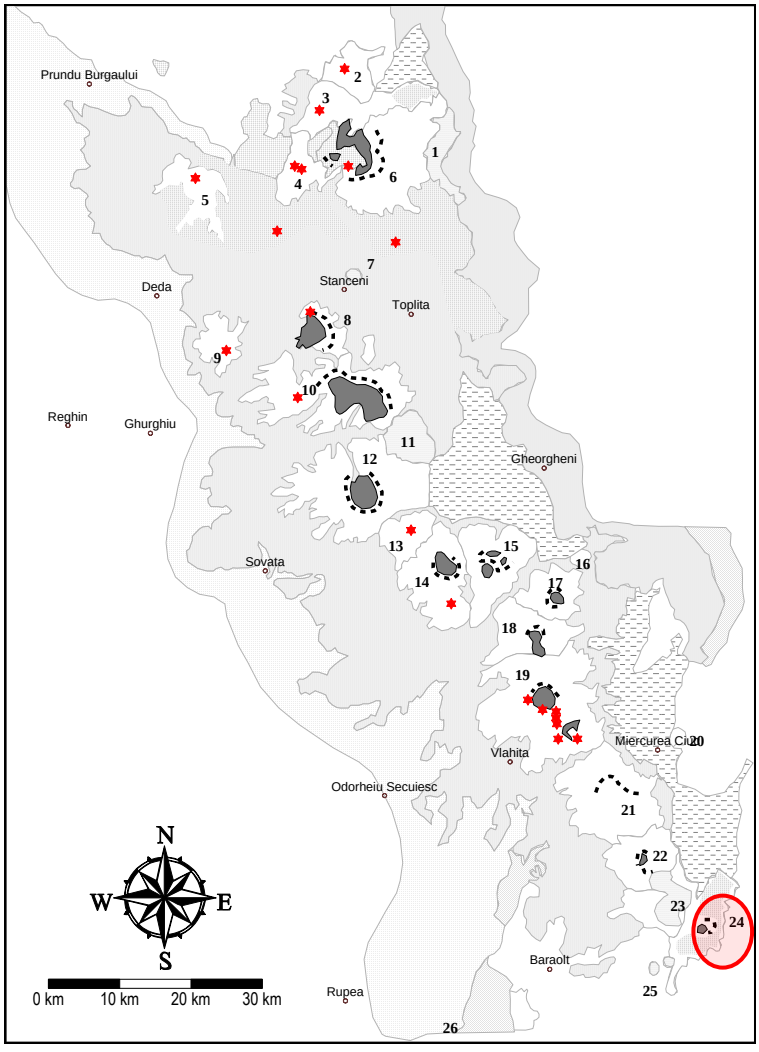

Fig. 4.3.1.1 Location of the Ciomadull volcano within the Neogene-Quaternary volcanism of East Carpathians.
1, Dragoiasa;2, Lucaciul; 3, Tămăul; 4, Rusca-Tihu; 5, Moldovanu; 6, Calimani; 7, Calimani Sud; 8, Jirca; 9, Obârşia; 10, Fâncel-Lăpuşna; 11, Bacta; 12, Seaca-Tătarca; 13, Borzonţ; 14, Ivo-Cocoizaş; 19, Vârghiş;
20, Sumuleu-Ciuc; 21, Luci-Lazu; 22, Pilişca; 24, Ciomadul; 25, Bicsad-Malnaş

4.3.1.1.1. Topography

Figure 4.3.1.2 presents a model of the topographic surface within the Ciomadul volcano area. The model has been obtained based on the 1: 100.000 maps of the Topographic Service of the Romanian Army.

The SURFER 8 software package (©Golden Software) has been use for visualisation. Visualisation parameters are as follows:

- Projection system: Stereo 1970
- Reference ellypsoid: WGS 1984
- Altitude datum: Sistem Marea Neagră 1975
- Grid size: 100 m
- 3D visualisation with illumination from SE
- Vertical asymouth 40 degrees
- Ortographic perspective

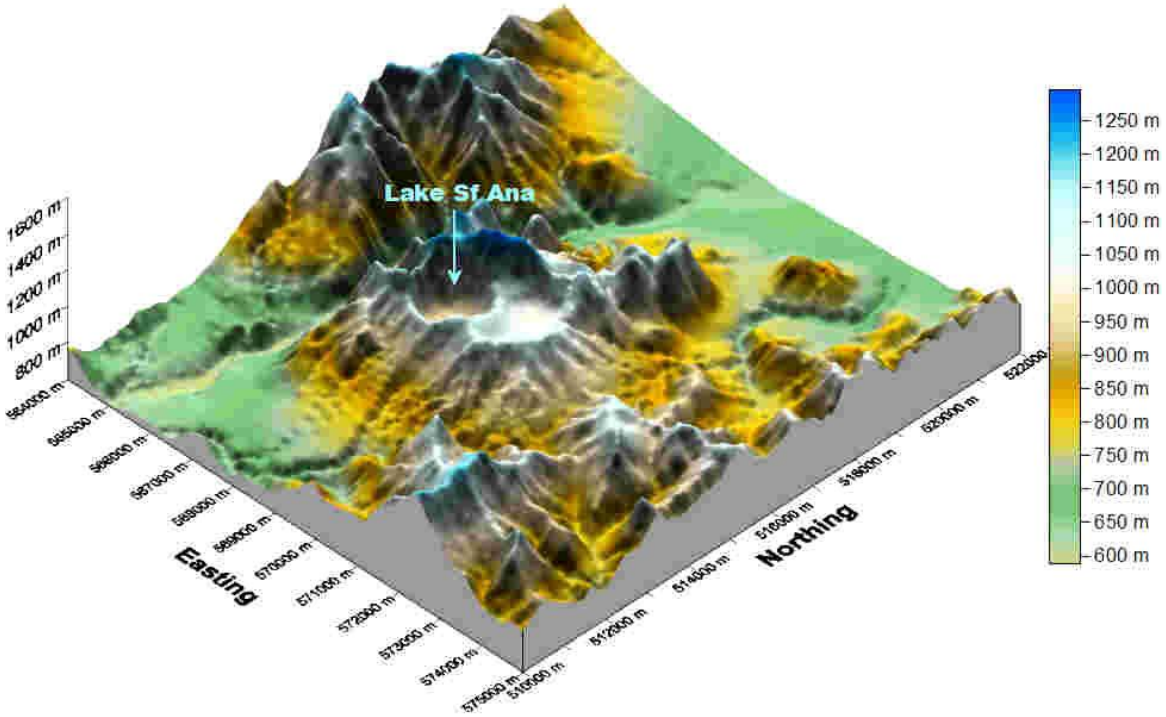

Fig. 4.3.1.2 Topography model of the Ciomadull volcano area

4.3.1.1.2. Geological setting

The simplified geological map presented in the figure 4.3.1.3 is based on Szakács et al. (2015) along with the position of an interpretative line that will be discussed later.

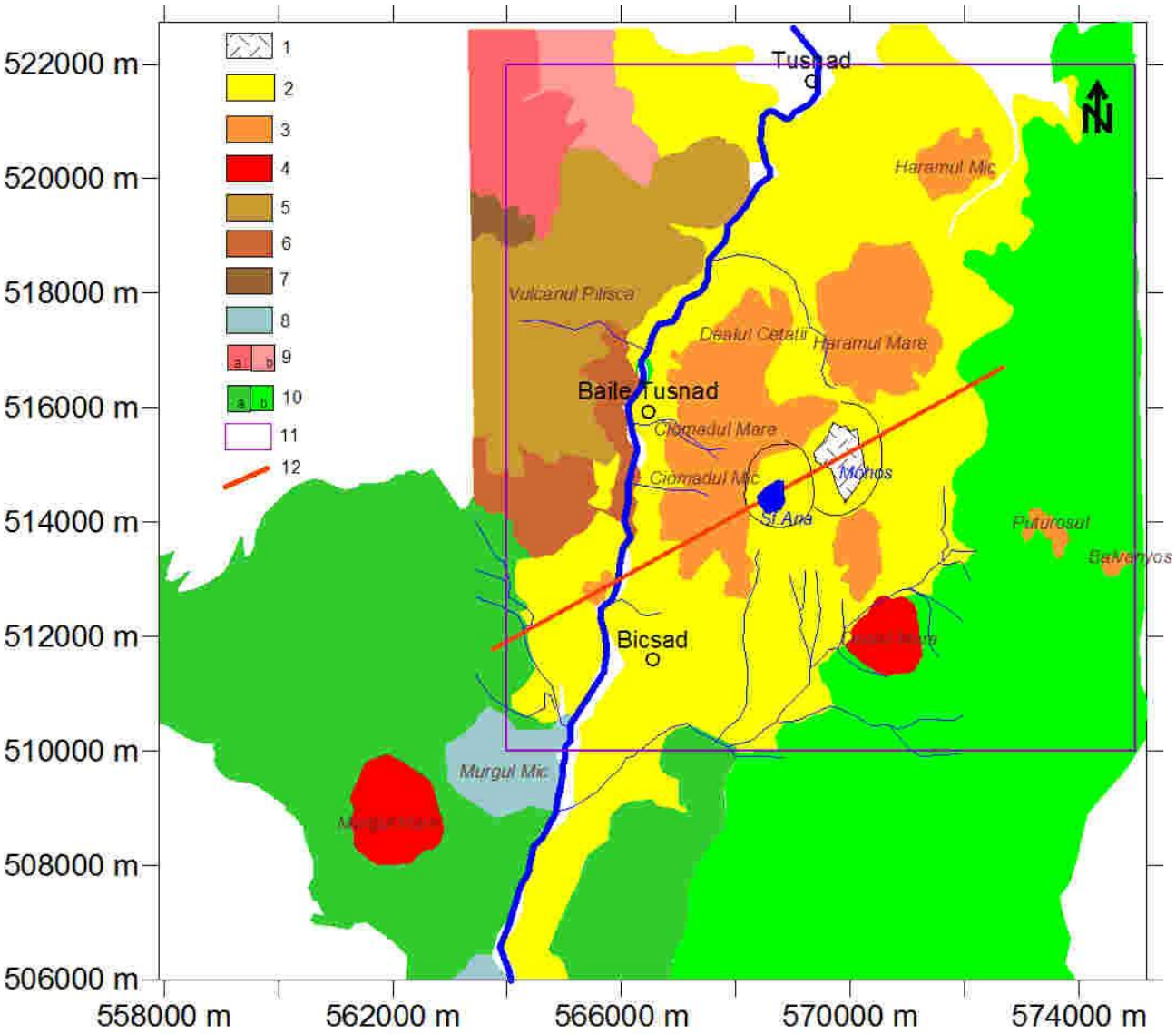

Fig. 4.3.1.3 Geological setting of Ciomadull volcano (according to Szakács et al., 2015)

1. Mohoș swamp; 2. Ciomadull volcano- vulcaniclastic deposits; 3. Ciomadull volcano – dacitic domes; 4. Dealul Mare and Murgul – andesitic domes; Pilisca volcano – dacitic and andesitic domes; 6. Pilisca volcano – andesic lavas with pyroxen and amphibol; 7. Pilisca volcano – basalt andesitic lava flows type Mitaci; 8. Bixad-Malnaș - shoshonitic domes; 9. Cucu volcano: **a.** Amphibol +/- biotit andesite; **b.** volcaniclastics; 10. Cretaceous flish deposits: **a.** Tithonic-Neocomian; **b.** Barremian-Albian;11.studied area; 12.2D interpretative line.

4.3.1.1.3. Gravity field

An image of the gravity field trend as the Bouguer anomaly pattern within the Ciomadull area is shown in figure 4.3.1.4.

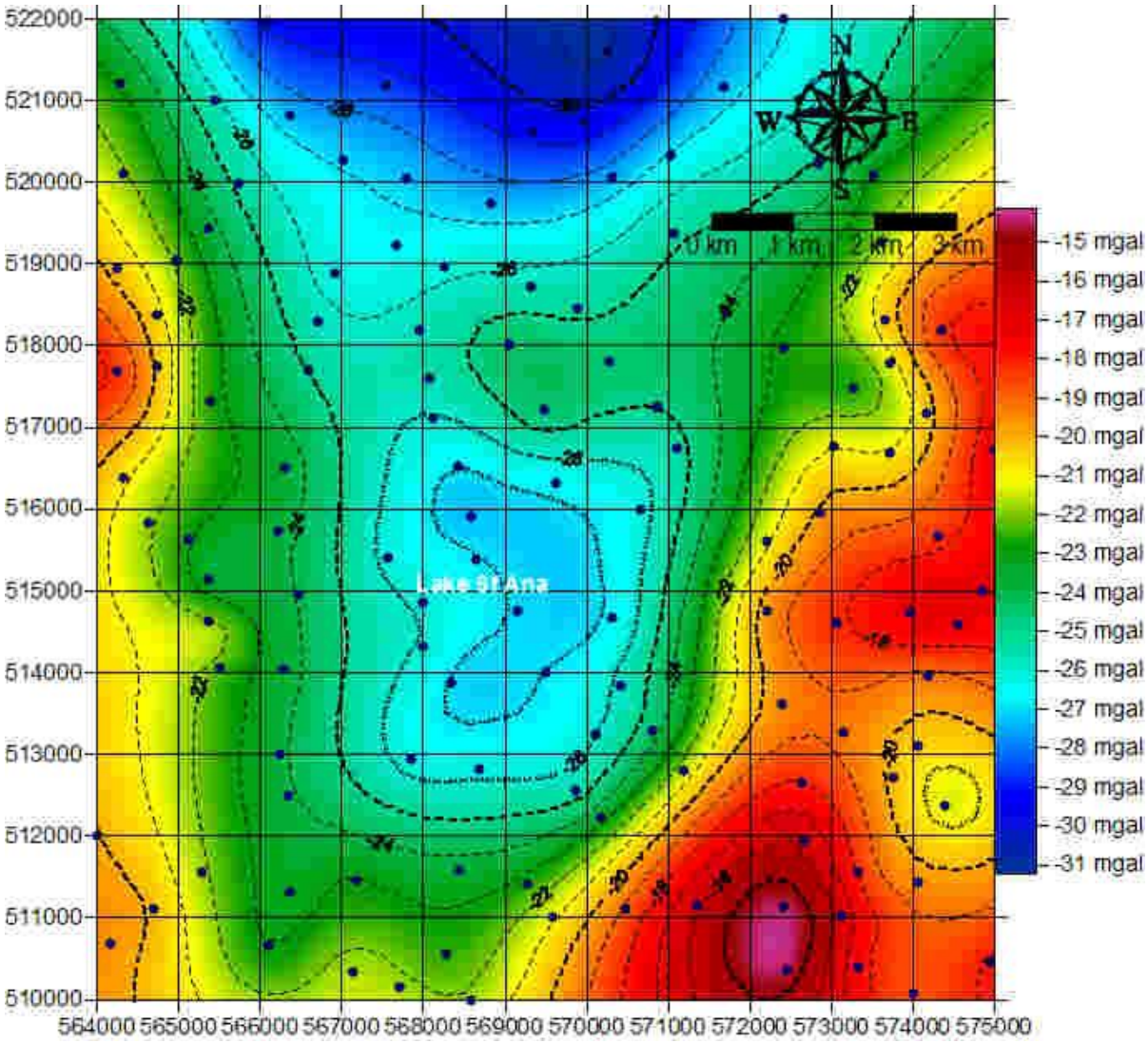

Fig. 4.3.1.4 Bouguer anomaly in the Ciomadull volcano and neighbouring area

The computing approach and representation has been chosen according to rules generally accepted in Romania:

- Gravity System: IGSN71 (International Gravity Standardization Network 1971).
- Reference field: Silva-Cassinis 1934 model
- Reference density: 2.20 g/cmc
- Bouguer anomaly computing radius: 20 km

Interpolating operator: Krigging

The size of the griding cell (0.5 km x 0.5 km) has been determined by the data coverage.

4.3.1.1.4. The geomagnetic field

The image of the geomagnetic field has been generated as the geomagnetic anomaly of the total intensity scalar (figure 4.3.1.5). To avoid topography bias, data were transferred to a horizontal plan at the altitude of 1300 m above the sea level.

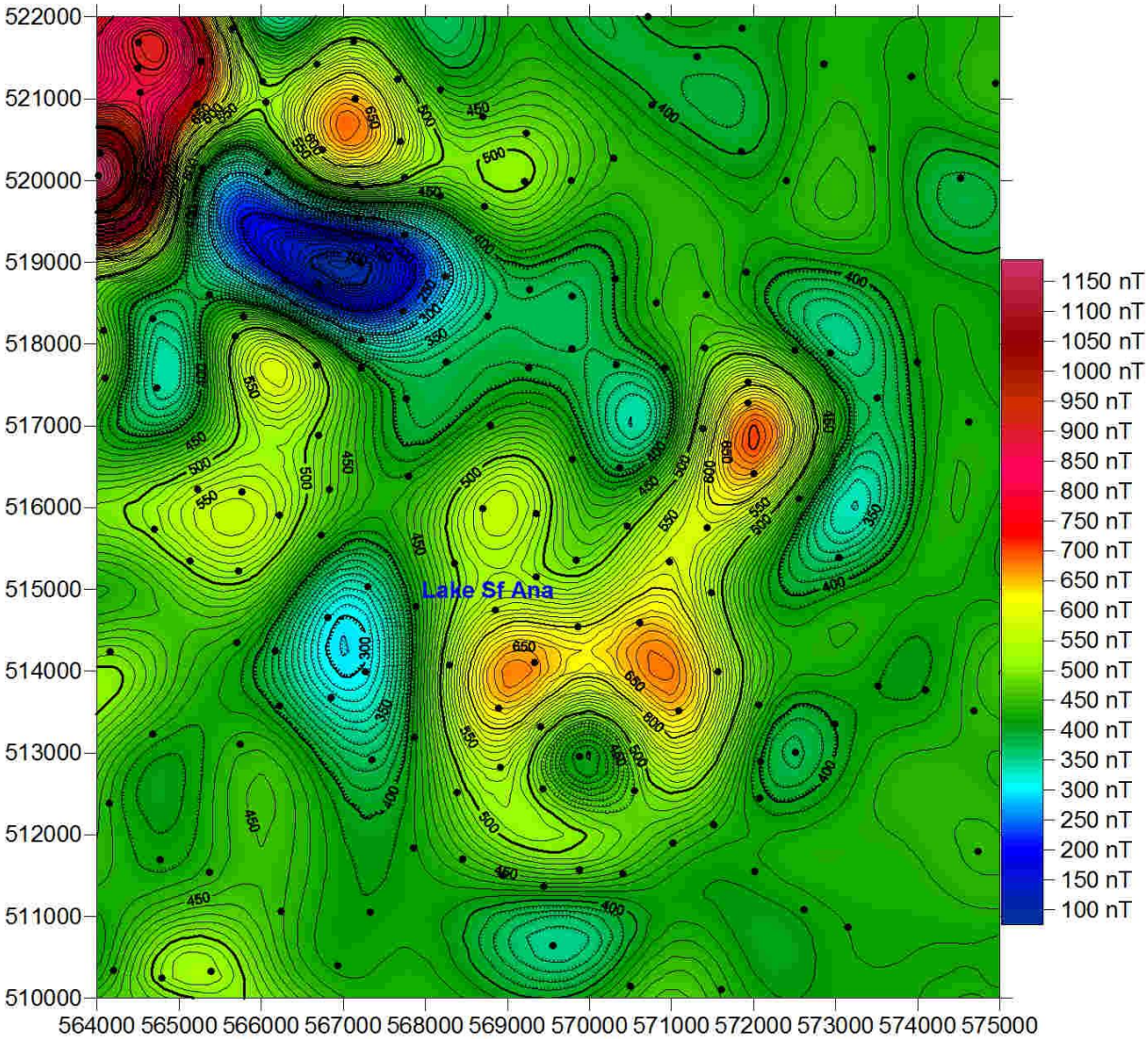

Fig. 4.3.1.5 Geomagnetic anomaly of the Ciomadull volcano at 1300 m above sea level

The computing approach and visualisation relies on the following parameters:

- Geomagnetic reference field: IGRF 12
- Magnetic contours interval: 10 nT
- Interpolating approach: Krigging
- Grid size: 0.5 km x 0.5 km

4.3.1.1.5 Rock physics

A synthetic lithostratigraphy column has been constructed based on the geological formation known in the area. Densities and magnetic susceptibility values, as determined on samples in the lab of the Solid Earth Dynamic Department, were added to each significant geological formation in this column (see table below).

PETROGRAPHY	No. of samples	Susceptibility (SIu)	Density (g/cmc)
ANDESITE	158	0.00017-0.109	2.02-2.94
BASALT	10	0.00302-0.156	2.66-2.82
WEATHERED BASALT	1	0.0642-0.0855	2.79
BASALT BOMB	1	0.055-0.139	2.06
BASALT TUF	2	0.0166-0.101	1.99-2.06
TUF	3	-0.0002 - 0.000194	1.92-1.96
CRYSTALOCLASTIC TUF	1	0.00017-0.0002	2
LIMESTONE	12	-0.00055 -0.00057	2.66-2.75
LIMELY SANDSTONE	4	0.00004-0.00118	2.39-2.54
POLYMICTIC CONGLOMERATES	2	0.00011-0.00152	2.56-2.62
MANTLE XENOLITH	1	0.0096-0.0137	3.14
NON-FIFFERENTIATED Cretaceous (K)	1416		2.59±0.13
LOWER Cretaceous	76		2.58±0.12
UPPER Cretaceous	1198		2.59±0.13

The table outlines the main potential sources of gravity and/or geomagnetic anomaly expected in the area that have been considered in the modelling process.

4.3.2. 3D MODELS OF THE GRAVITY AND GEOMAGNETIC SOURCES IN THE STUDIED AREA OBTAINED BY AN ITERATIVE APPROACH

4.3.2.1 General considerations

The modelling process has been obtained by using the software package GM-SYS on the OASIS (© GEOSOFT Ltd) platform for forward modelling, but also the inversion package „VOXI Earth Modelling" provided on-line by Geosoft to Geosoft beneficiaries .

The GM-SYS package may allow for 2D, 2 ½ D, and 3D forward modelling of the sources of the gravity and geomagnetic anomalies previously mentioned.

As most of the computing rutines, GM-SYS Profile Modelling is based on the Talwani algorithms (Talwani et al., 1959 for gravity modelling and Talwani & Heirtzler, 1964 for geomagnetic sources). As reality has clearly demonstrated the limitations of the 2D approach, 3D algorithms become more common, benefiting of the increasing computing power of the new computers. The GMSYS – 3D package perform the numerical modelling required for 3D models of the gravity and geomagnetic sources with the help of the Fourier transform. The spectral algorithms are mainly based on the works of Parker (1973) and Oldenburgh (1974), improved later by various authors. The GM-SYS 3D modelling package along with the routine MAGMAP Filtering™ , working in the frequency domain, are based on Parker (1973) and Blakely (1995).

Recent advances have implemented a powerful tool in numerical modelling: inversion of gravity and geomagnetic data with the software package VOXI Earth Modelling, based on PARASOL, the inversion engine designed by Dr. Robert G Ellis for Geosoft Ltd . The power and speed of this package relies on the usage of parallel computing clusters. Geosoft Ltd offers to its beneficiaries the on-line access to a powerful computing centre with the possibility to store the solution for a limited time in the cloud (Microsoft Windows Azure).

4.3.2.2 Main steps in obtaining numerical models

4.3.2.2.1 2D forward modelling approach

The first step in obtaining the in-depth structural solutions was the construction of the informative 2D simulation models. Even if the volcanic forms are generally far from behaving as 2D structures, the methodology has been applied for providing the first information on the gravity and geomagnetic sources hidden in depth. In this approach, rock physics information, as obtained on samples from the study area, played an important role for constraining the modelling solutions in the absence of well data or other constraints. Some hydrothermal and a few structural data in the neighbourhood of Tusnad Bai indicated unusually high geothermal gradients (up to 200-400°C/km) in the vicinity of the surface, while lower values are known deeper (Radulescu et al.1981; Peter, 1984, Mitrofan, 2000). Based on this information, it has been considered that Curie point is above 5000 m in the area, fact that limits in depth the extent of our geomagnetic models. Neither gravity data are able to provide deeper information because of the limited extent of the study area that do not allow for distinct manifestation of the long-wave effects.

As we mentioned previously, the 2D forward modelling has been performed in the Solid Earth Dynamic Department by employing the software GM-SYS Profile Modelling run on the OASIS Montaj platform. The modelling was an iterative process, approaching step-by-step to solution. For instances, figure 4.3.2.3 shows the first results when the run used an assumed geological section based on the current knowledge on the area. The rock physics model has been designed based on the average lab determinations performed on samples from outcrops in the studied area.
As it can be seen, the geophysical effects produced by the currently accepted model on the underground structure do not lead to a satisfactory solution.

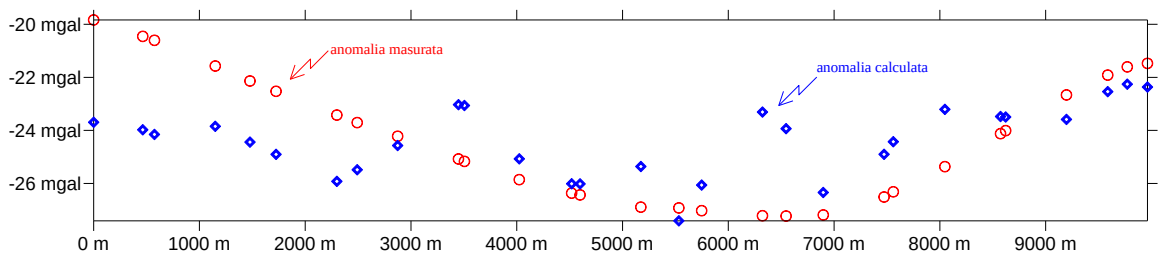

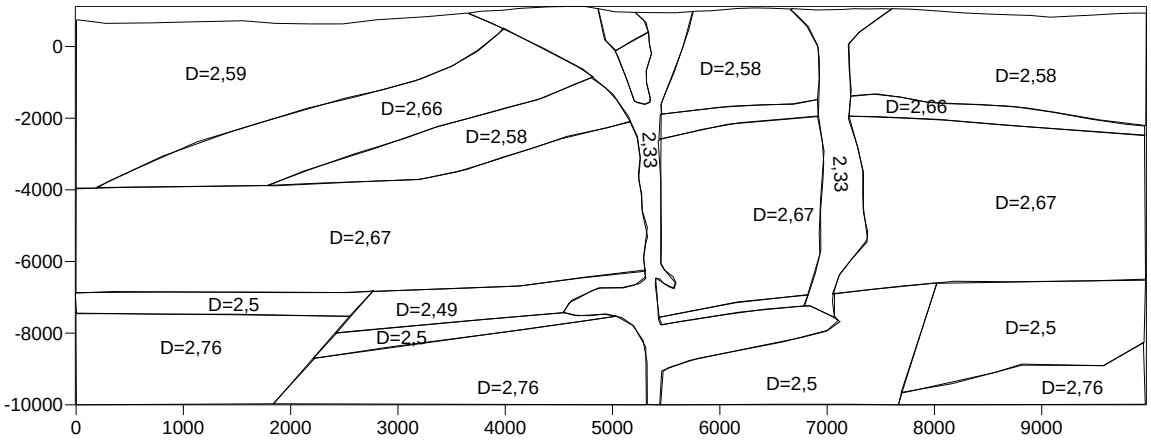

Fig. 4.3.2.3 First attempt to model the underground structure in the Ciomadull volcano area

The large differences between the observed and predicted gravity effect of the assumed geological structure with assigned rock physical densities as determined in the laboratory, are the result of differences between our current knowledge and geological reality.

Based on numerous iterations, when both geometry of the hidden structures and values of the densities were changed, we have finally succeeded to satisfactorily accommodate the predicted gravity effect with the observed gravity anomaly (figure. 4.3.2.4).

Still, we have to emphasize that even in such a favourable case, the obtained solution may not represent the geological reality at least for two major reasons:
- the inadequate 2D approach of a three-dimensional structure
- the inherent ambiguity of the solution in the interpretation of the potential field.

The similar results obtained by integrating gravity and geomagnetic modelling may slightly reduce ambiguities, but cannot eliminate them.

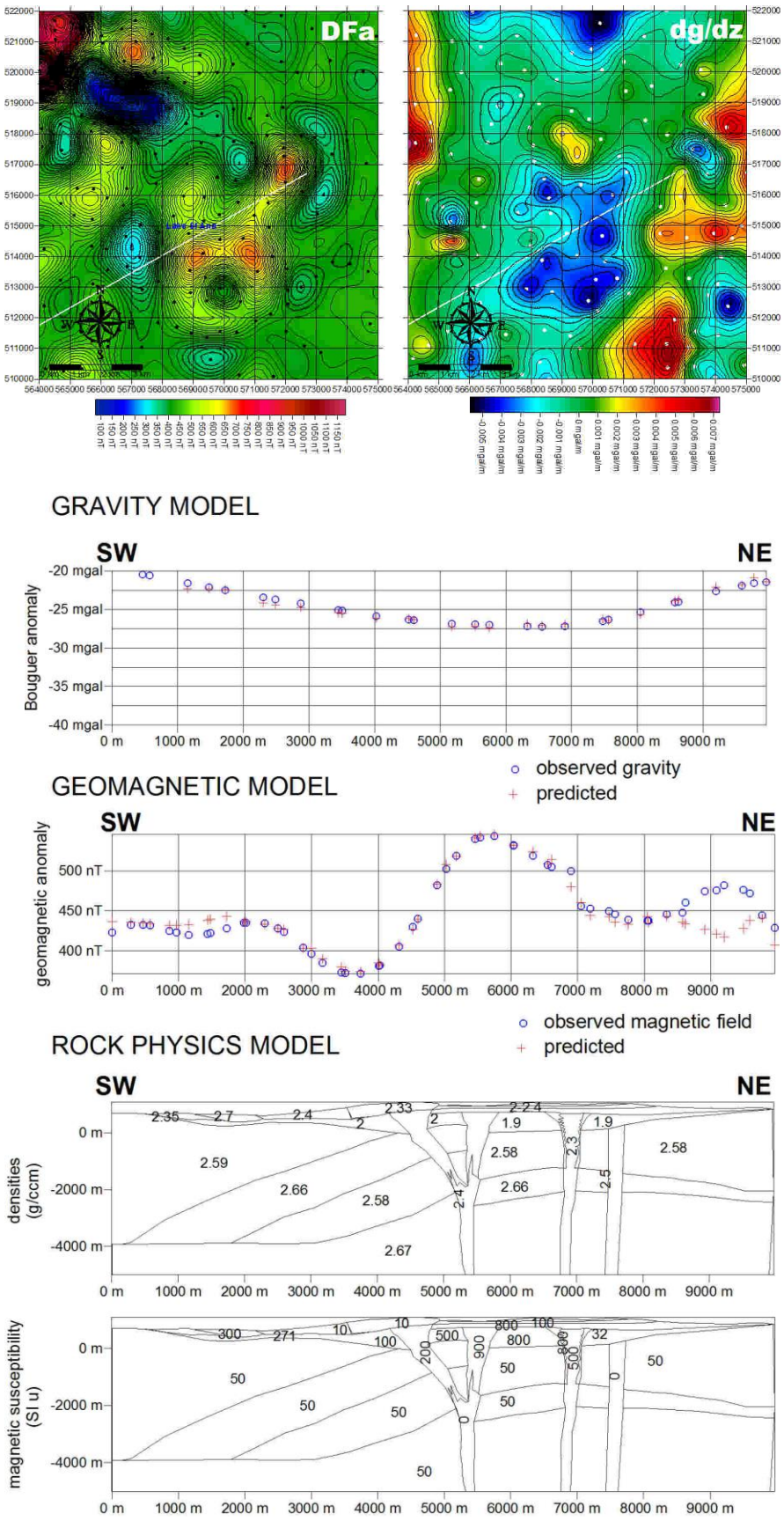

Figura 4.3.2.4 Joint 2D modelling of the gravity and geomagnetic data along a line crossing the Ciomadull volcano area.
Above: gravity and geomagnetic anomaly maps with location of the interpretative line
Below: Observed versus predicted gravity and geomagnetic fields along with structural and rock physics models of the underground

4.3.2.2.2. 3D forward modelling

Figure 4.3.2.5 shows images of the gravity and geomagnetic anomaly in the Ciomadull volcano area along with a 3D model of topography.

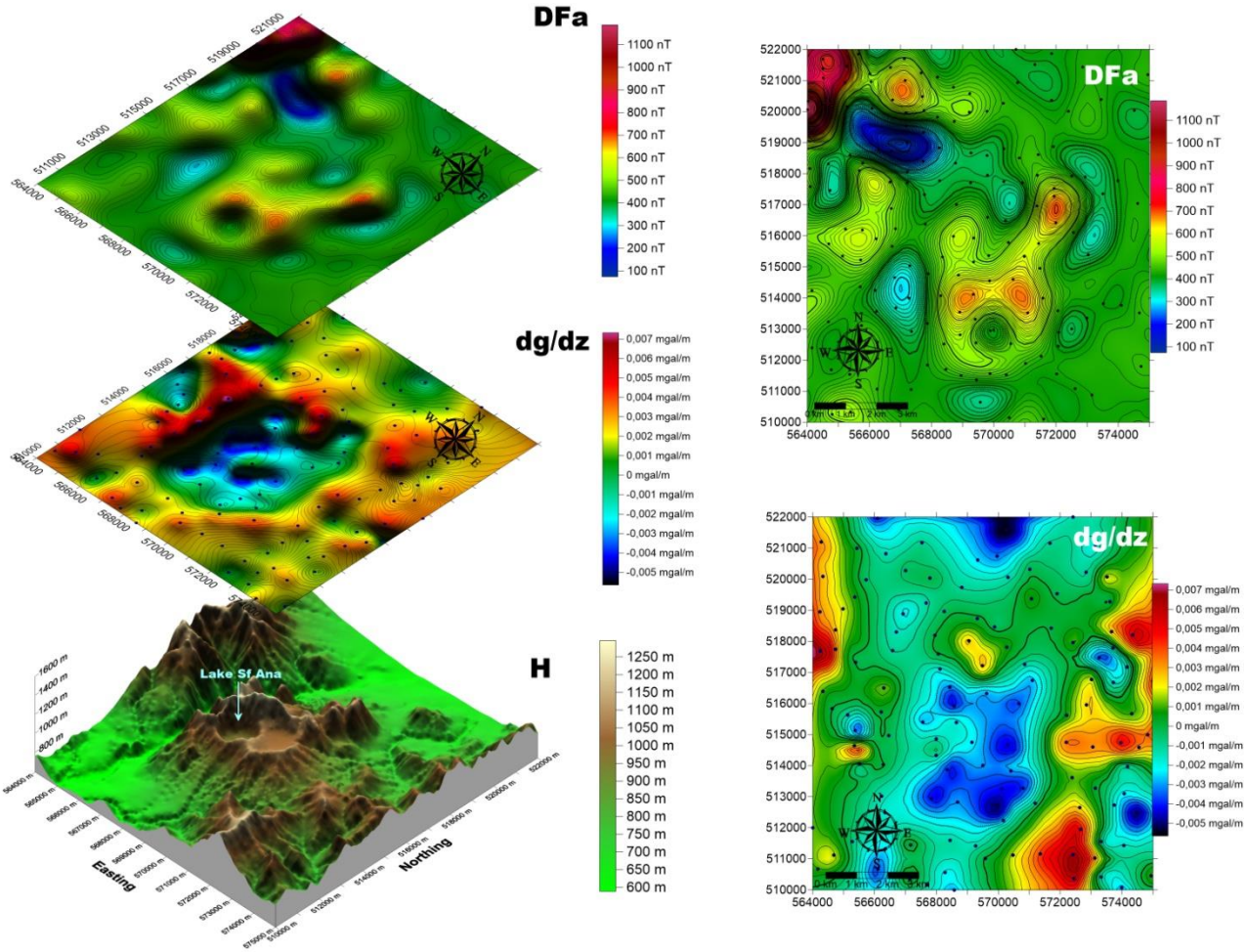

Fig. 4.3.2.5 Input data for the 3D forward modelling approach: gravity, geomagnetic anomaly and topography

The 3D forward modelling approach started from a rather simplified model of reality: a homogeneous lithospheric bloc overlain by topography (Fig. 4.3.2.6).
Several attempts to model its gravity effect have been made by progressively changing the considered block average density.

Figs. 4.3.2.7- 4.3.2.2.10 illustrate the obtained results.

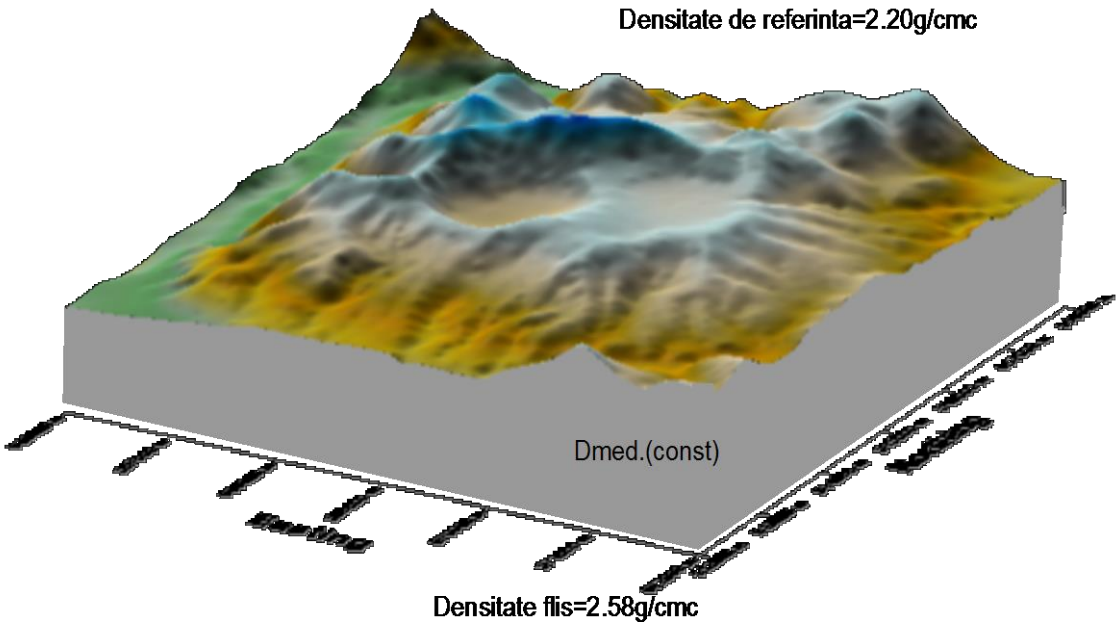

Fig. 4.3.2.6 Simulation environment for computing the effect of the lithospheric homogeneous block confined between topography and a plan situated at sea level overlying the Cretaceous flysch of constant density 2580 kg/m^3

By progressively changing the average density of the upper (homogeneous) block, several results have been obtained as shown in the following figures (Fig. 4.3.2.7 to 4.3.2.10).

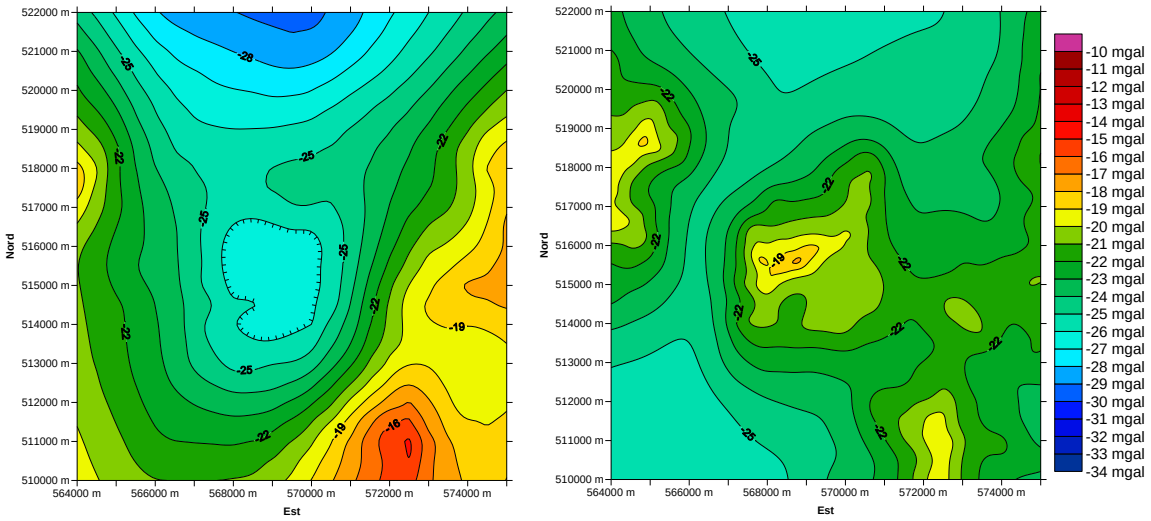

Fig. 4.3.2.7 Observed (left) versus predicted (right) Bouguer anomaly on a horizontal plan located at 1300 m above the sea level as computed for an average density of 2580 kg/ km^3

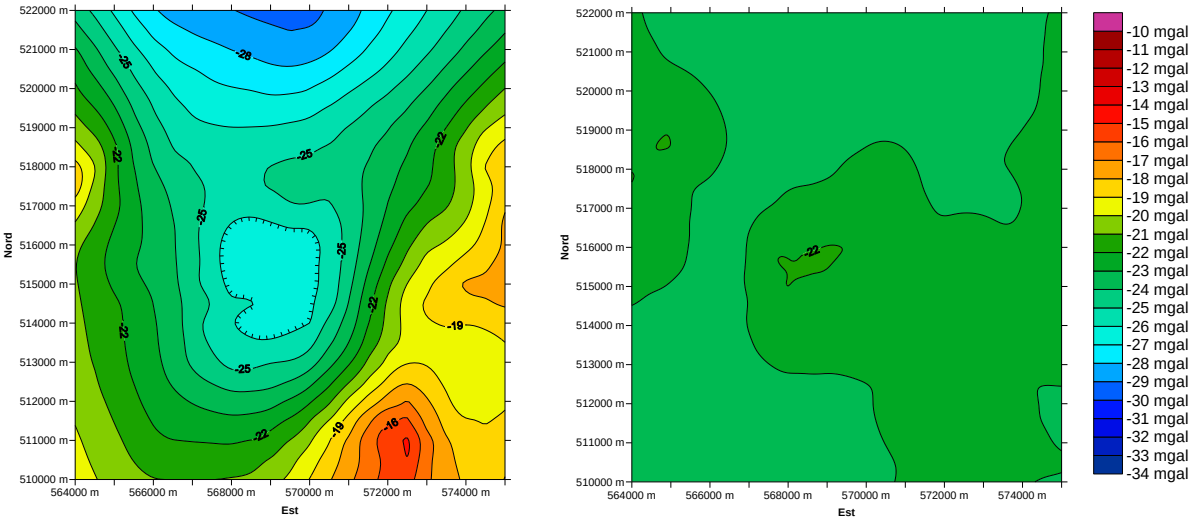

Fig. 4.3.2.8 Observed (left) versus predicted (right) Bouguer anomaly on a horizontal plan located at 1300 m above the sea level as computed for an average density of 2300 kg/ km^3

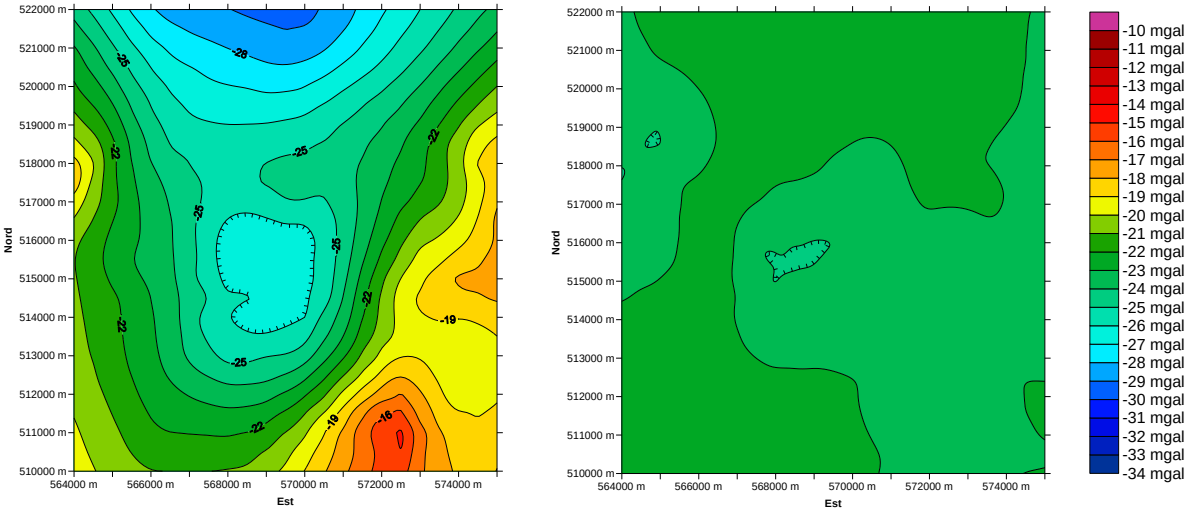

Fig. 4.3.2.9 Observed (left) versus predicted (right) Bouguer anomaly on a horizontal plan located at 1300 m above the sea level as computed for an average density of 2100 kg/ km^3

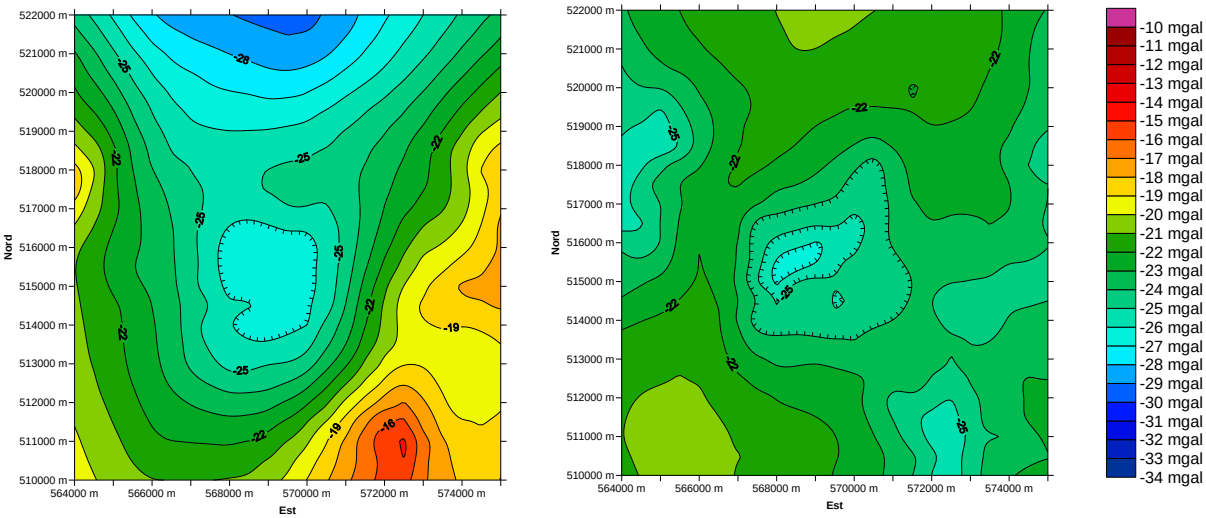

Fig. 4.3.2.10 Observed (left) versus predicted (right) Bouguer anomaly on a horizontal plan located at 1300 m above the sea level as computed for an average density of 1900 kg/ km^3

As expected, the simplified starting structure could not offer appropriate solutions to

the problem. Therefore, the next step in the approach was to complicate the geometry of underground structures by implementing lateral changes in the lithosphere density. After multiple attempts, the most appropriate solution has been obtained for a density change between 1,9 g/cm^3 and 2,2 or 2,3 g/cm^3, by taking into consideration the lateral effect of the Cretaceous flysch zone, well developed in the ESE part of the study area (with an average density of 2.58 g/cm^3.

The results are shown in Fig. 4.3.2.11.

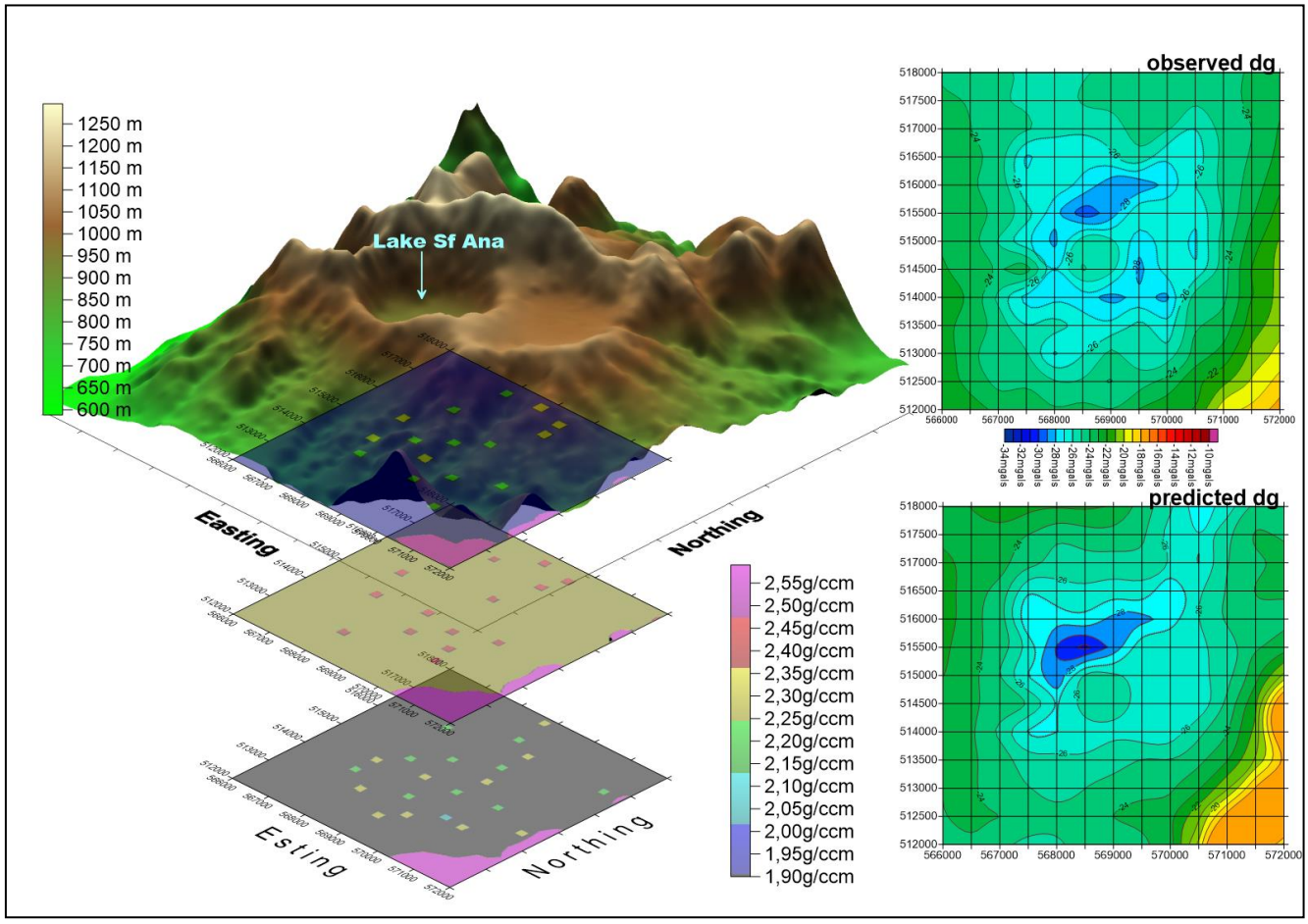

Fig. 4.3.2.11 Preliminary models of the underground structure beneath the Ciomadull volcano as obtained by 3D forward modelling

On the left side a 3D topography model of volcano is presented, along with several horizontal cross-sections showing the lateral change of density. The three cross-sections are located at depths corresponding to altitudes of1000 m, 800 m and 500 m. It should be noted the presence of several local density contrasts, probably caused by the presence of dyke systems. On the right, observed versus predicted gravity effects.

4.3.2.3 Geophysical models of the Ciomadul volcano as inferred from the inversion approach

The final attempt for deciphering the in-depth structure of the Ciomadul volcano has been performed by using the inversion approach provided by the help of the software package **VOXI Earth Modelling,** provided on-line by Geosoft Ltd to its beneficiaries. The software has been remotely run on a HPCC hired by the owner, using the parallel computing system for speeding up computing processes. The modelling solution has been obtained within several steps, by advancing from simple to complex structures.

4.3.2.3.1 Version zero

The first version of the model has been obtained within an inversion approach free of any constraint (Fig. 4.3.2.3.1).

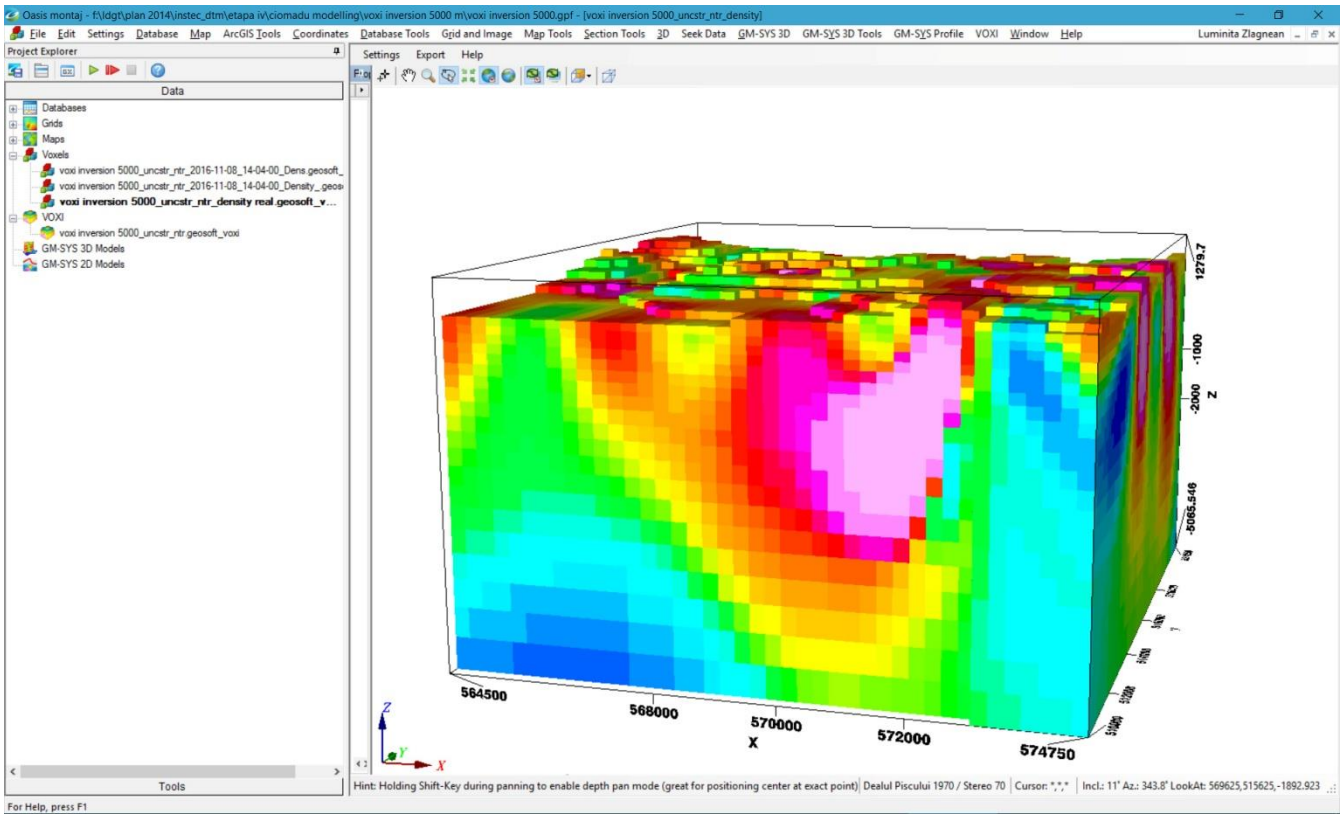

Fig. 4.3.2.3.1 Screen capture from the application VOXI Earth Modelling showing a 3D model of the density distribution beneath the Ciomadul volcano
The computing mesh: horizontal grid cell: 250 m x 250 m; vertical step variable
Coordinate system Stereo 1970. Altitude datum: Black Sea 1975
Axis X towards E; axis Y towards N; Z positive up
Visualisation parameters: horizontal angle 315 grade; vertical azimuth: 22 grade

4.3.2.3.2 Advanced version

The next step in obtaining the 3D model of density distribution has used a residual gravity anomaly as obtained by removing a first order gravity trend. The result has improved the signal due to gravity sources located closer to the observation point, mainly within the modelling environment.

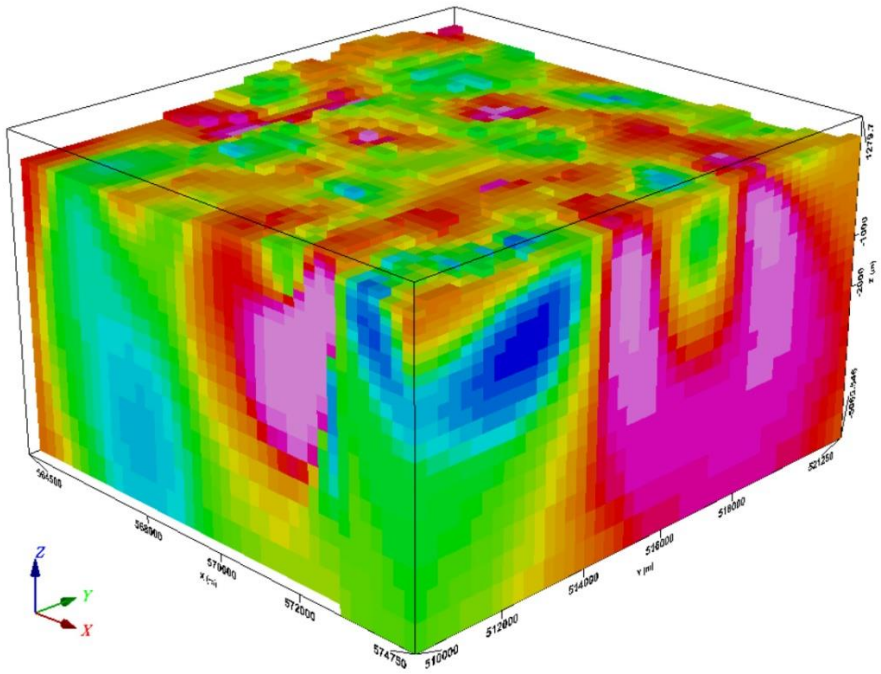

Fig. 4.3.2.3.2 3D density model beneath the Ciomadul volcano as inferred from the inversion of the detrended Bouguer anomaly
The computing mesh: horizontal grid cell: 250 m x 250 m; vertical step variable
Coordinate system Stereo 1970. Altitude datum: Black Sea 1975
Axis X towards E; axis Y towards N; Z positive up
Visualisation parameters: horizontal angle 315 grade; vertical azimuth: 22 grade

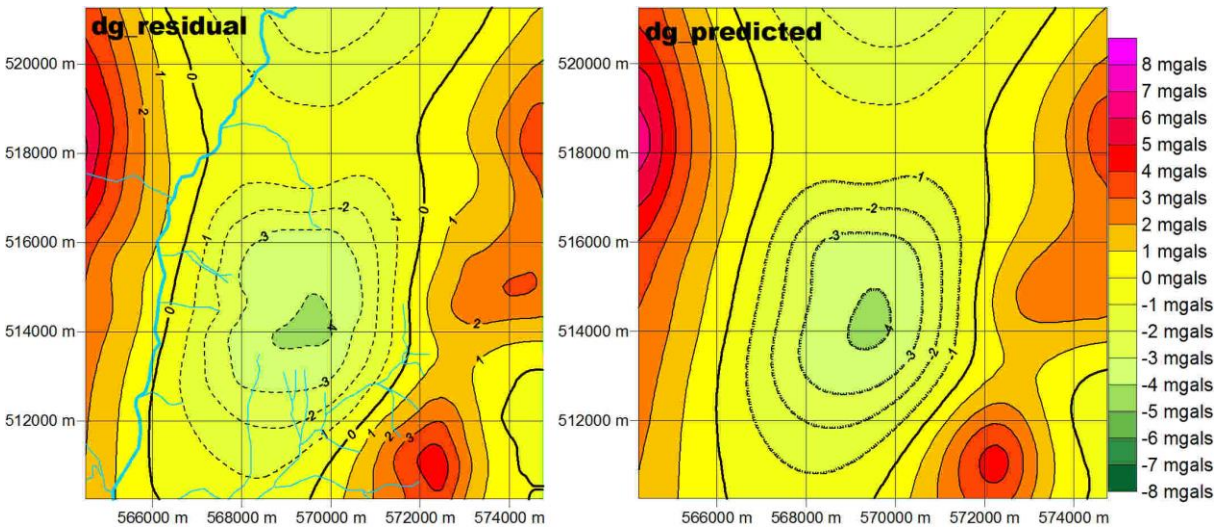

Fig. 4.3.2.3.3 Observed versus predicted gravity effect produced by the density model obtained through inversion

The misfit between observed and predicted models is below 0.5 mgal, representing the accuracy threshold of the observed data (Fig. 4.3.2.3.4)

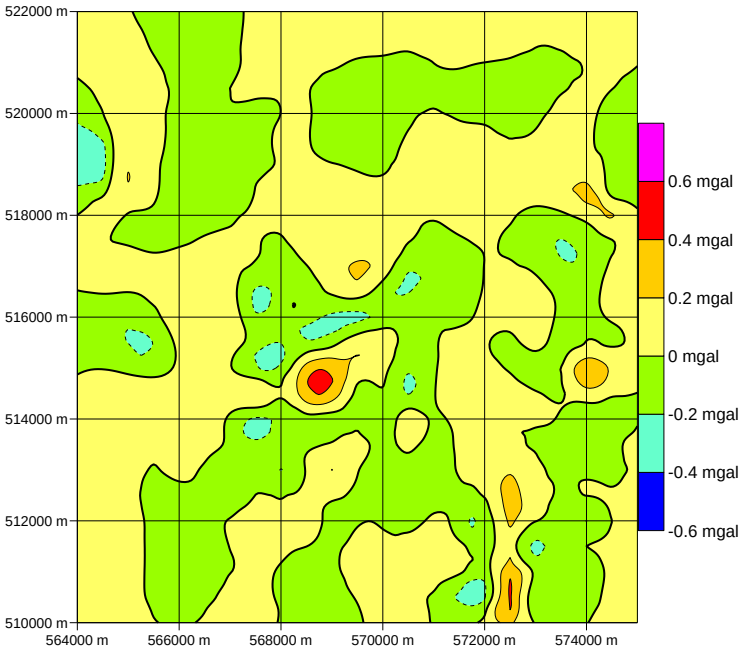

Fig. 4.3.2.3.4 The misfit between observed and predicted gravity effect produced by the density model obtained through inversion

For better understanding the created 3D model, figures 4.3.2.3.5 – 4.3.2.3.8 shows it from four spatial perspectives.

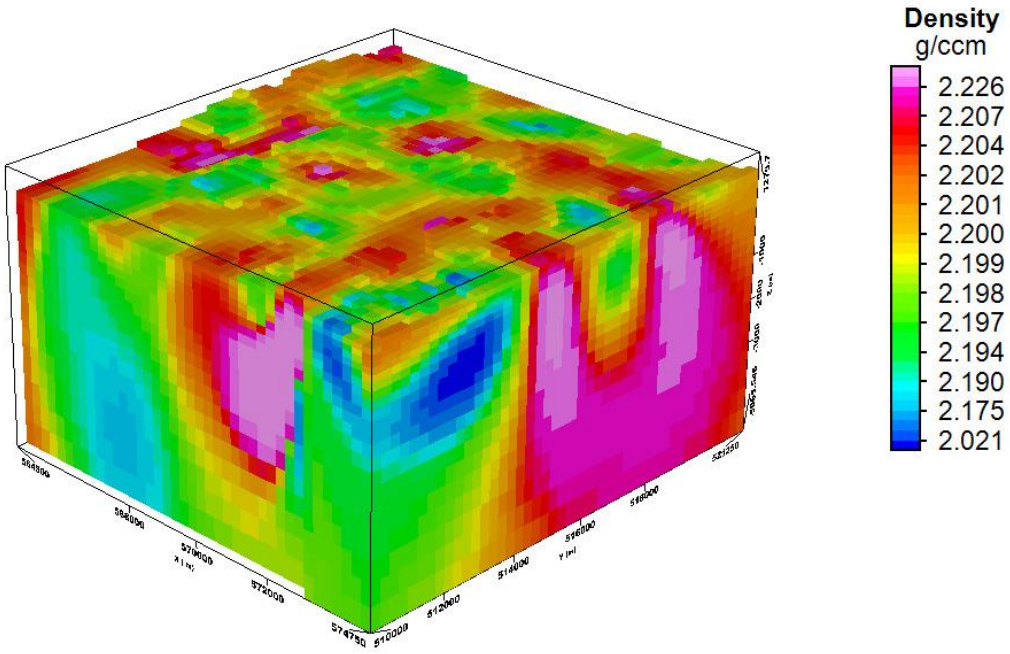

Fig. 4.3.2.3.5. 3D density model of Ciomadul Vulcano as seen from a SE perspective
The computing mesh: horizontal grid cell: 250 m x 250 m; vertical step variable
Coordinate system Stereo 1970. Altitude datum: Black Sea 1975
Axis X towards E; axis Y towards N; Z positive up

Visualisation parameters: horizontal angle 315 grade; vertical azimuth: 22 grade

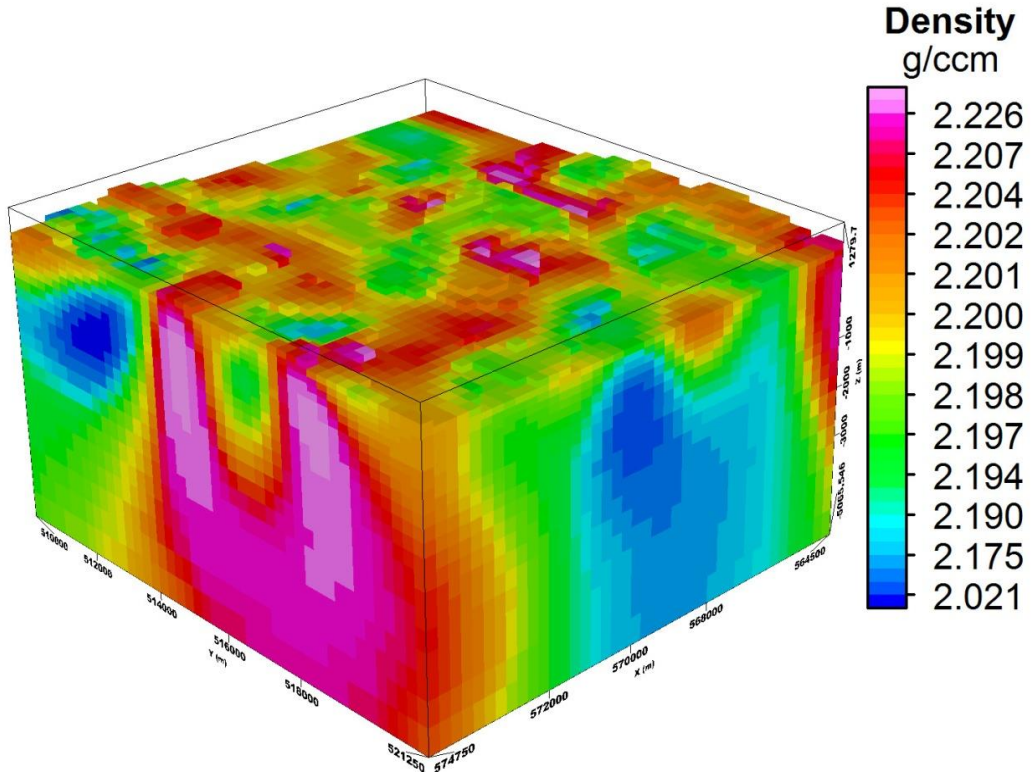

Fig. 4.3.2.3.6 3D density model of Ciomadul Vulcano as seen from a NE perspective

The computing mesh: horizontal grid cell: 250 m x 250 m; vertical step variable
Coordinate system Stereo 1970. Altitude datum: Black Sea 1975
Axis X towards E; axis Y towards N; Z positive up
Visualisation parameters: horizontal angle 225 grade; vertical azimuth: 22 grade

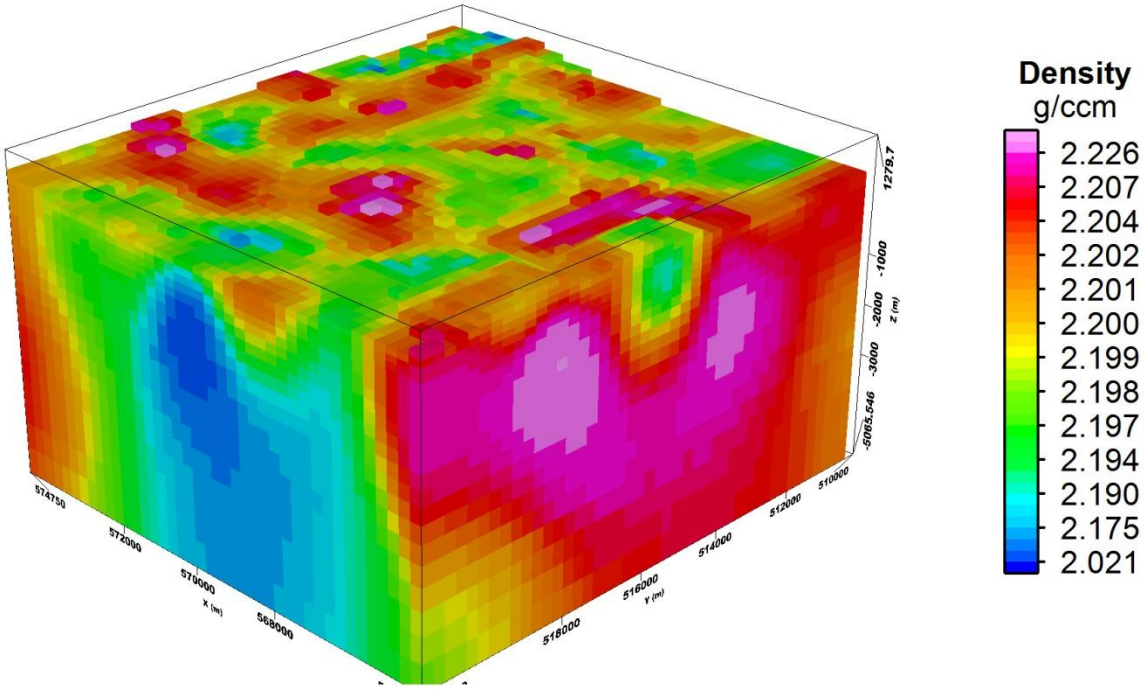

Fig. 4.3.2.3.7 3D density model of Ciomadul Vulcano as seen from a NW perspective

The computing mesh: horizontal grid cell: 250 m x 250 m; vertical step variable
Coordinate system Stereo 1970. Altitude datum: Black Sea 1975
Axis X towards E; axis Y towards N; Z positive up

Visualisation parameters: horizontal angle 135 grade; vertical azimuth: 22 grade

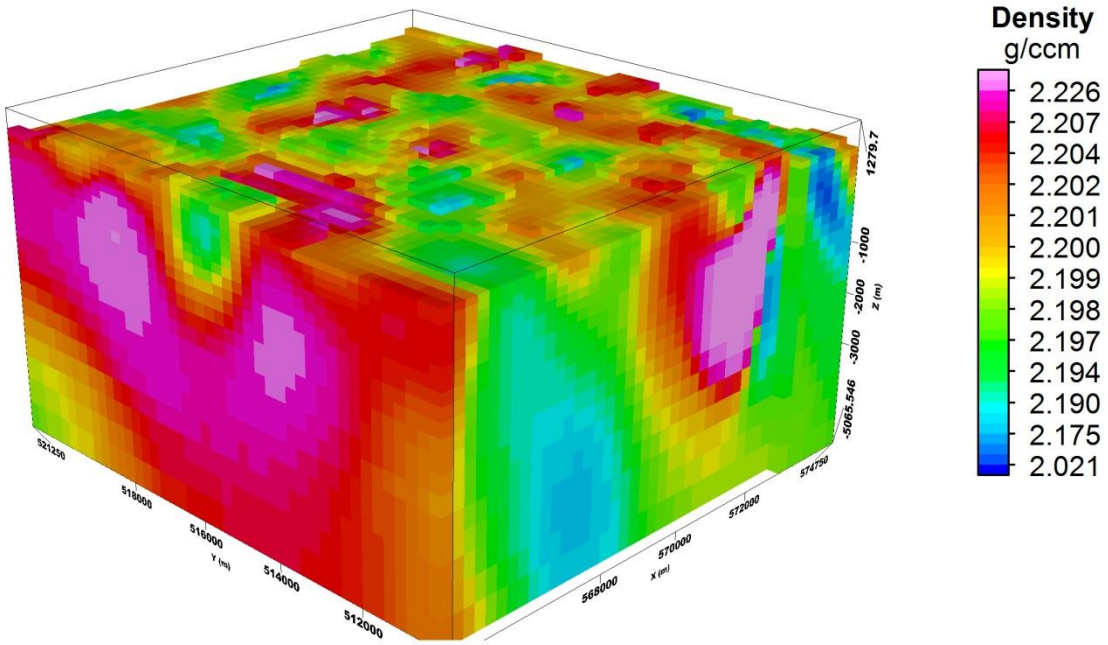

Fig. 4.3.2.3.8 3D density model of Ciomadul Vulcano as seen from a SW perspective
The computing mesh: horizontal grid cell: 250 m x 250 m; vertical step variable
Coordinate system Stereo 1970. Altitude datum: Black Sea 1975
Axis X towards E; axis Y towards N; Z positive up
Visualisation parameters: horizontal angle 45 grade; vertical azimuth: 22 grade

We also have determined and visualised some horizontal cross-sections throughout the model, located at various depths (Figure 4.3.2.3.9). It should be noted that overall, highest values occur in the eastern part of the model, where only sedimentary deposits crop out, while the western part is dominated by lower densities.

The presence of a low-density anomaly below -1000m (relative to sea level) beneath the Lake Sf Ana and Mohoş swamp is also noteworthy. The anomaly is progressively widening till ~ -3000m and then decreases at depths beneath -4000m.

We shall return to this effect later on, in the attempt of interpreting the results.

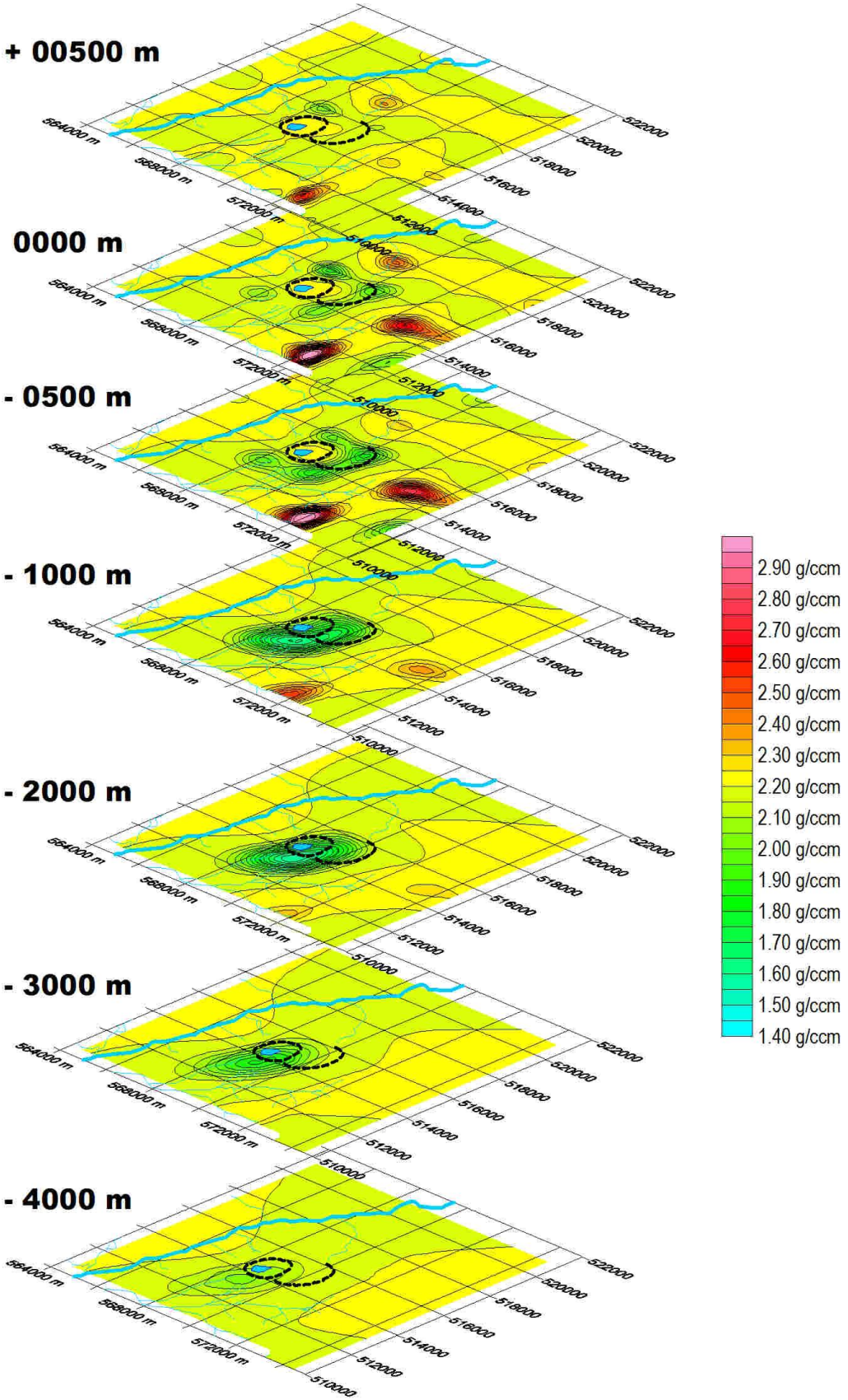

Fig. 4.3.2.3.9. Horizontal cross-sections through the density model beneath Ciomadul volcano

The computing mesh: horizontal grid cell: 250 m x 250 m; vertical step variable
Coordinate system Stereo 1970. Altitude datum: Black Sea 1975
Axis X towards E; axis Y towards N; Z positive up
Visualisation parameters: horizontal angle 315 grade; vertical azimuth: 22 grade

4.3.3. GEOLOGICAL INTERPRETATION OF THE 3D DENSITY MODELS OBTAINED THROUGH NUMERICAL SIMULATION

Behind the three-dimensional density model of the Ciomadul volcano stands a geological reality reflected by the geophysical parameter. In the attempt to decipher the geological background hidden behind the geophysical information, we started from the comparison with surface geological data (e.g. Szakács & Seghedi, 1986; 1989; Szakács et al., 2015)

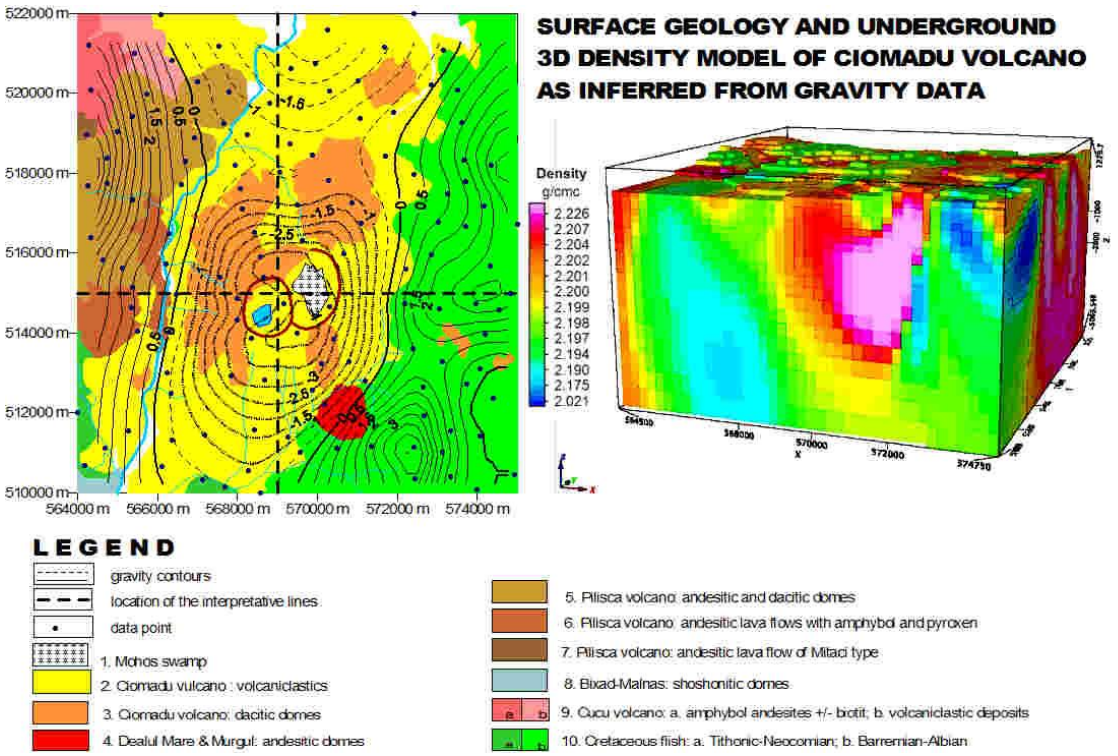

Fig. 4.3.3.1 Geological map of the Ciomadul volcano area (modified after Szakács et al, 2015) and 3D model of density beneath the volcano
The computing mesh: horizontal grid cell: 250 m x 250 m; vertical step variable
Coordinate system Stereo 1970. Altitude datum: Black Sea 1975
Axis X towards E; axis Y towards N; Z positive up
Visualisation parameters: horizontal angle 335 grade; vertical azimuth: 18 grade

The three-dimensional image is difficult to interpret as a whole, most of the information being masked by the modelling environment wedges. For exploring the interior of the model, we prepared horizontal and vertical cross-sections (providing more intuitive images).

These interpretative lines have been chosen along various directions, all crossing the central part of volcano, the Sf. Ana Lake. The following figures show the results obtained. The first section strikes W-E by crossing in the neighbourhood of the lake (Fig. 4.3.3.2).

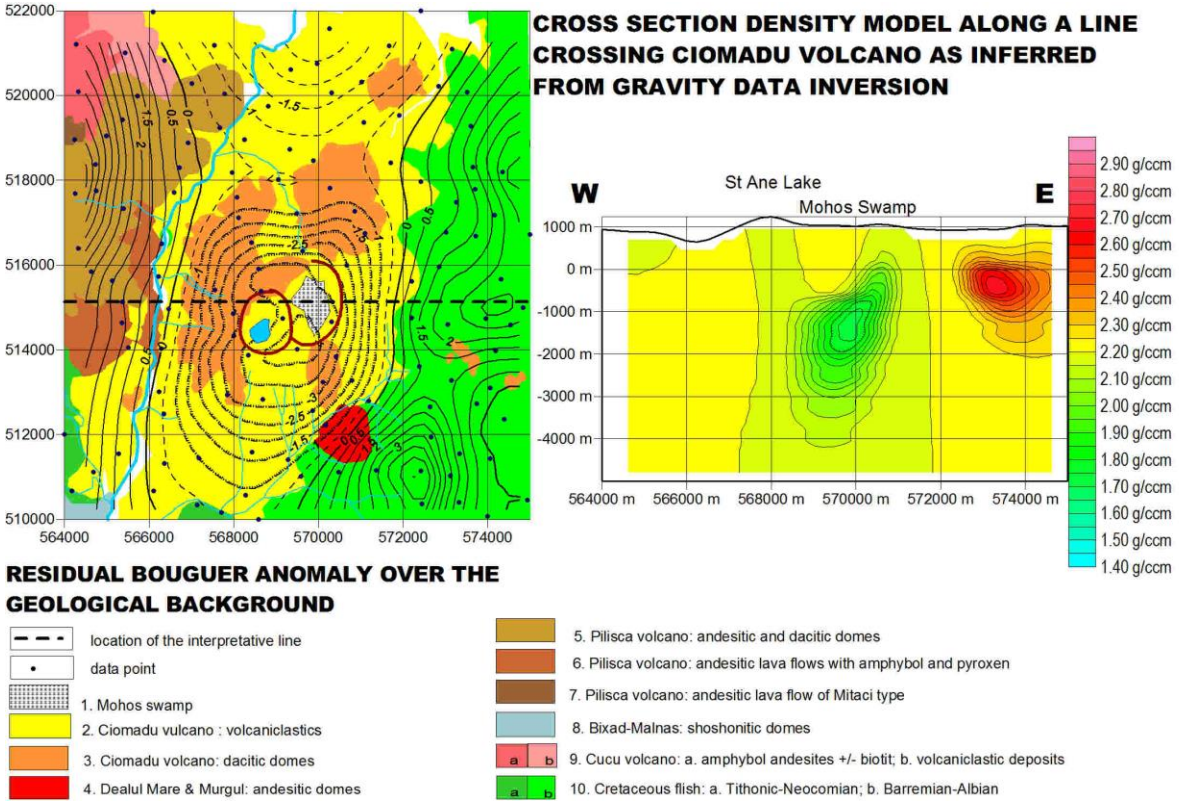

Fig. 4.3.3.2 Geological sketch of Ciomadul volcano area (modified after Szakács et al, 2015) and cross-section through the 3D density model along a line striking W-E

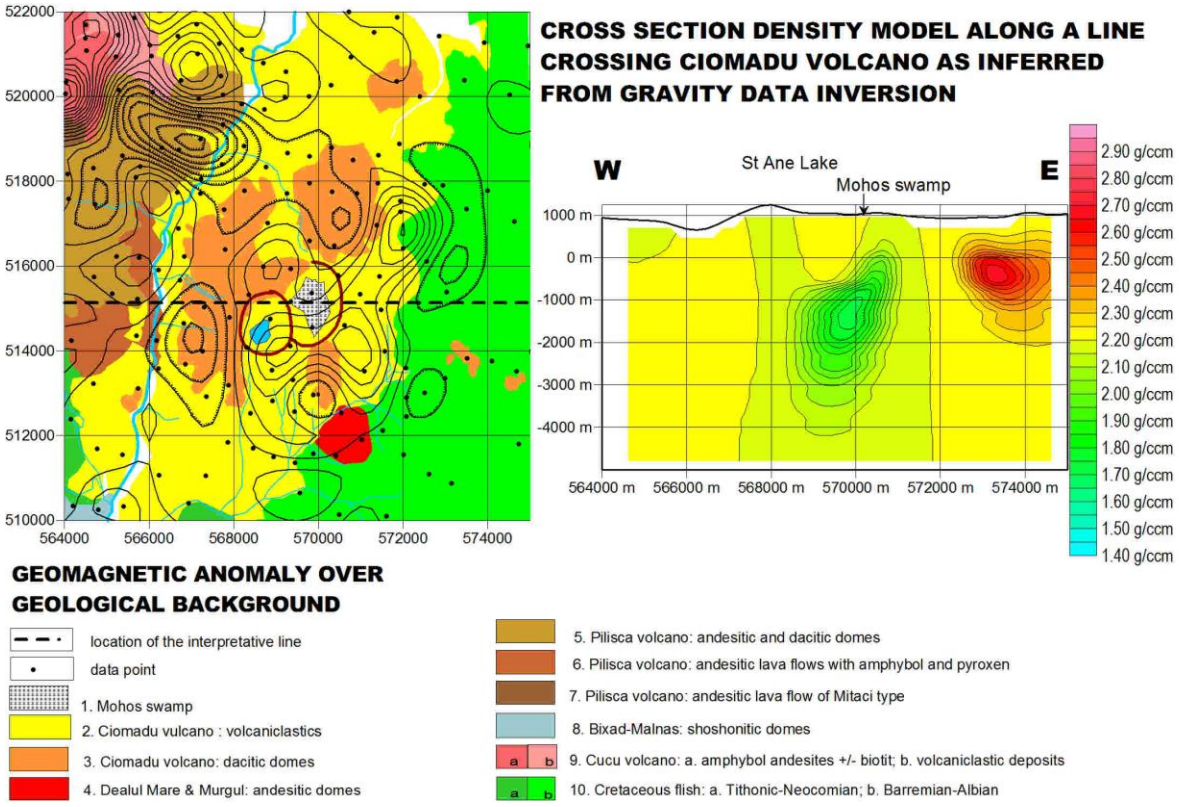

Fig. 4.3.3.3 Geomagnetic anomaly vs geological background in the Ciomadul volcano area and a vertical cross-section through 3D density model striking W-E

The repartition of densities along the line reveal a lower density zone located somewhere beneath the Lake Sf Ana and Mohos swamp. The unusual low density values start at more than -1000 m below Mohos swamp and at more than -2000m beneath Lake Sf Ana. The anomaly may be observed down to more than -4000 m below the sea level but, given the limits of the gravity approach, could extended even deeper. The geomagnetic data clearly show the presence of local geomagnetic anomalies within the Sf Ana - Mohoş area, that likely reflect the presence of some volcanic rocks (like andesite) hidden beneath a sedimentary cover. The geomagnetic anomalies appear south of Ciomadul volcano, in agreement with the location of the revealed density effect. However, it is worth mentioning that none of the volcanic rocks encountered at the surface does exhibit such a low density, even if slightly weathered. Consequently, the idea of the existence of some hot rocks in depth should be taken into consideration. The high dip of the anomalous zone between the Ciomadul volcano should be also noticed: it suggests a possible connection between the magma access ways and some reverse faults that resulted by tectonic processes during the East Carpathians Alpine overthrust.

A second interpretative line crosses Lake Sf Ana directly, running from South to North (Fig. 4.3.3.4). Figure 4.3.3.5 presents the density cross-section comparative with the geomagnetic information in the area. As it can be observed, this time the mass deficit revealed along the first line is dipping almost vertical beneath the lake and develops from the altitude of -1000m below sea level, down to more than -4000 m.

The anomaly is complicated by a secondary branch towards north that correlates very well with the local geomagnetic anomaly occurring in the area of Ciomadul Mare peak.

It is also worth mentioning the narrowing of the anomaly at its lower part, that seems to suggest the existence of a feeding channel in the area, but the information should be prudently treated because it occurs in the marginal part of the model, strongly affected by biasing due to signal truncation.

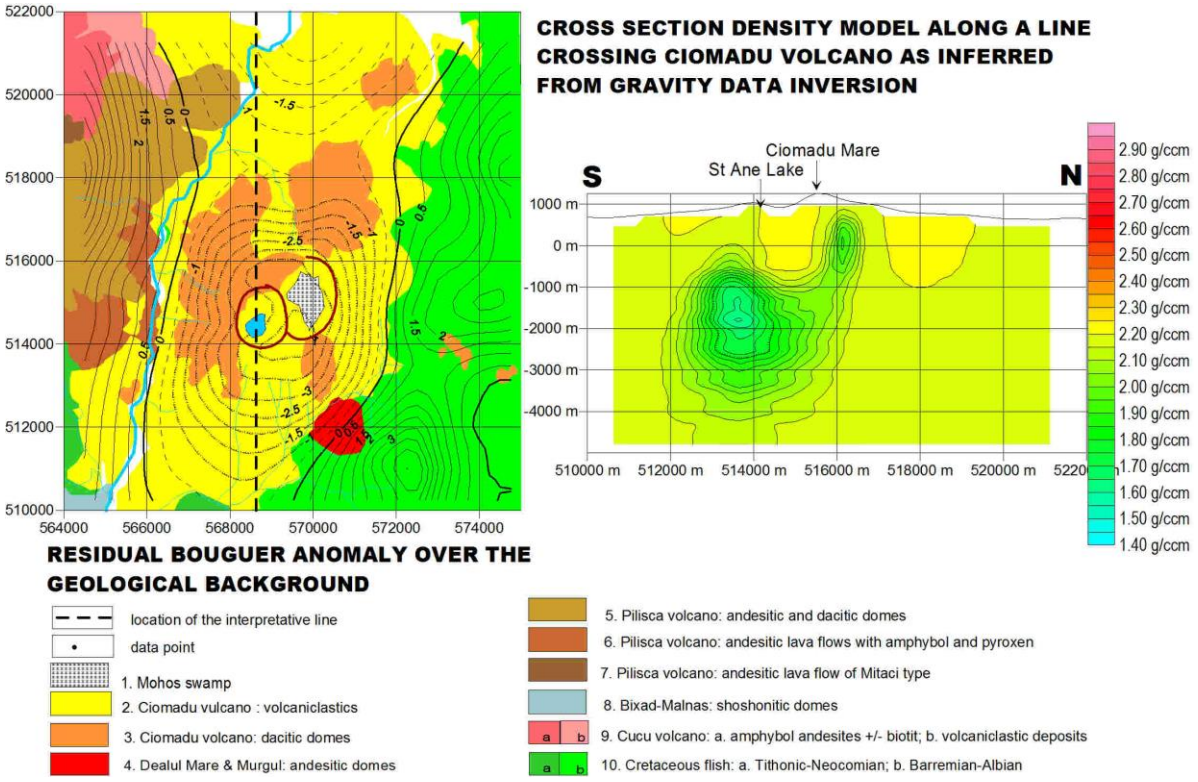

Fig. 4.3.3.4 Geological sketch of the Ciomadul volcano area (modified after Szakács et al, 2015) and cross-section through the 3D density model along a line striking N-S

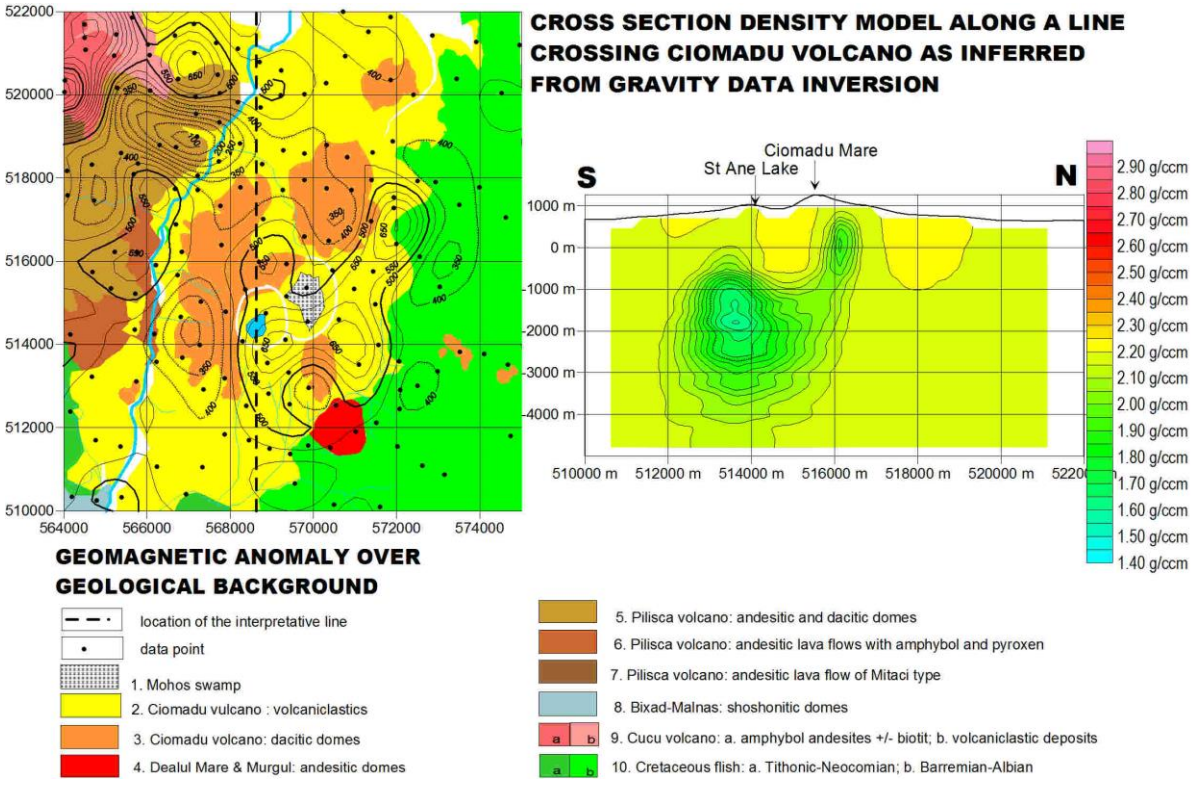

Fig. 4.3.3.5 Geomagnetic anomaly vs geological background in the Ciomadul volcano area and a vertical cross-section through 3D density model striking N-S

A third interpretative line runs SW-NE (fig. 4.3.3.6 şi 4.3.3.7). The results confirm assumptions made on the other lines.

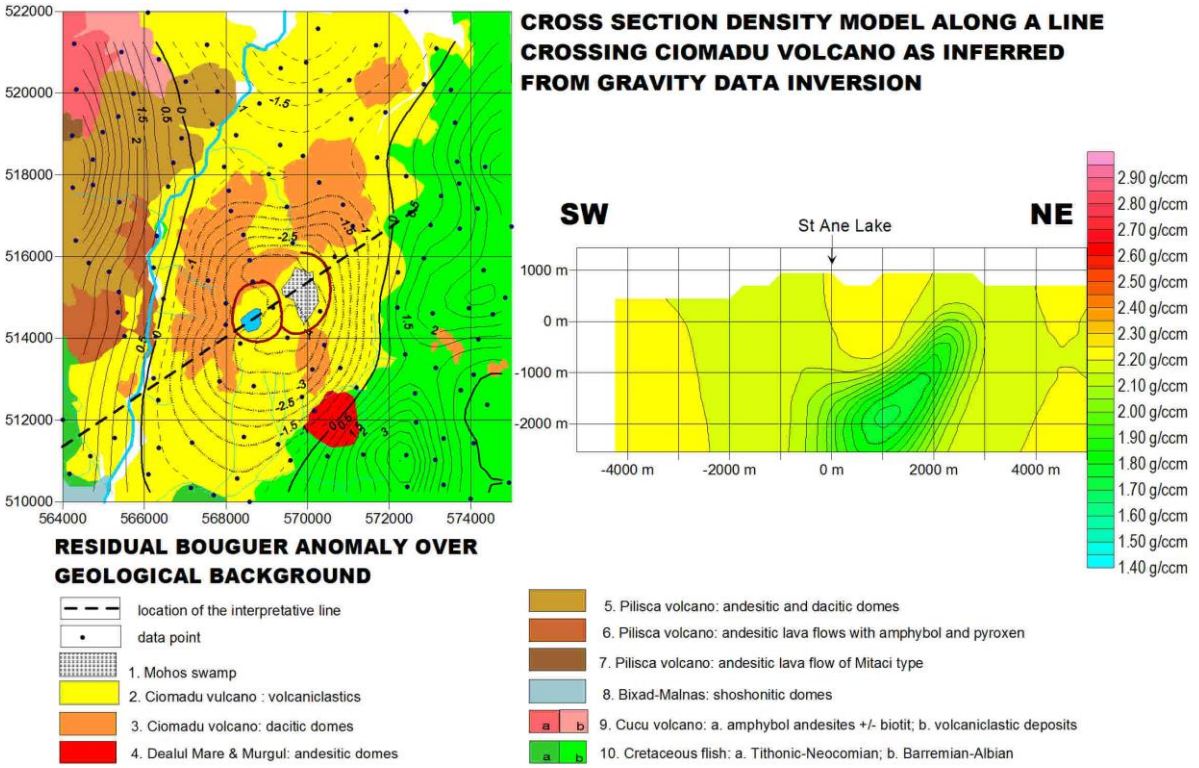

Fig. 4.3.3.6 Geological sketch of the Ciomadul volcano area (modified after Szakács et al, 2015) and cross-section through the 3D density model along a line striking SW-NE

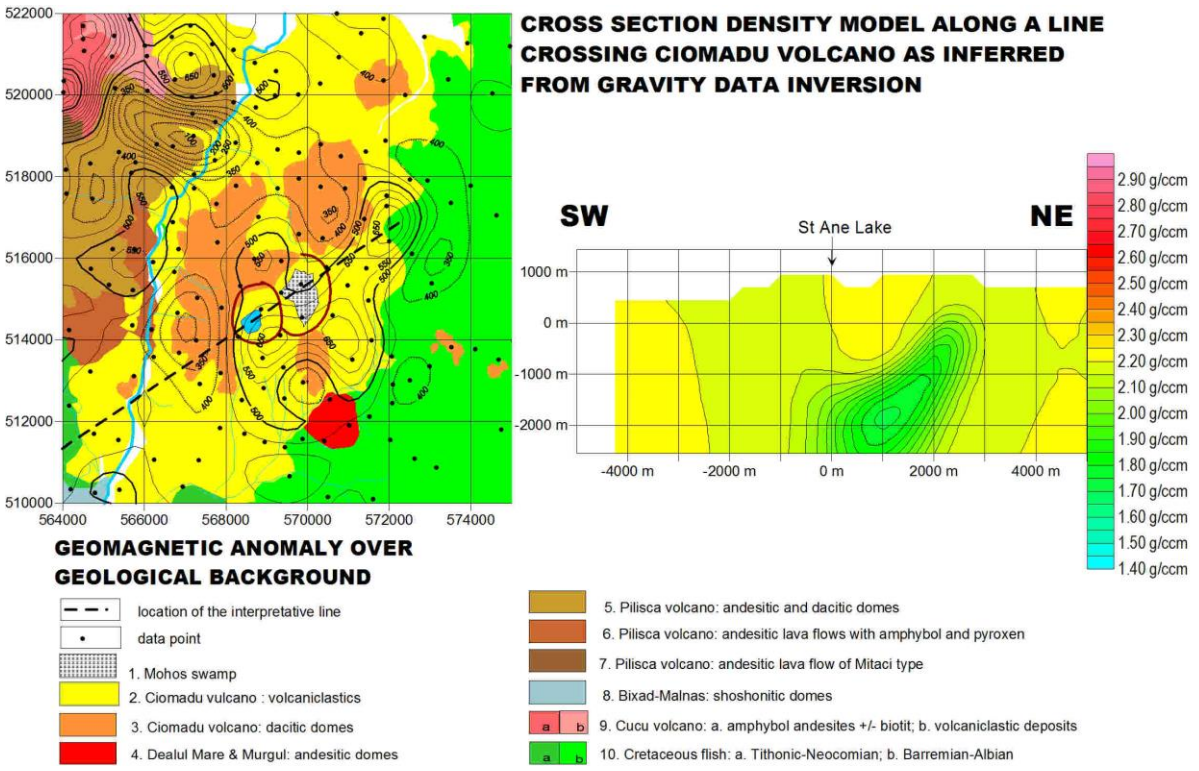

Fig. 4.3.3.7 Geomagnetic anomaly vs geological background in the Ciomadul volcano area and a vertical cross-section through 3D density model striking SW-NE

Therefore, the main idea explaining the density anomaly would be the presence of some hot rocks „reservoir" in depth, beneath Lake Sfânta Ana and Mohos swamp. The relative shallow location (at about 2000 m below the surface) of the top of the anomalous zone renders the existence of melted rocks improbable. They would need much higher temperatures involving important geothermal effects at the surface, which is not observed. However, the high values of the geothermal gradients westward recorded in wells drilled near Tuşnad Bai (+400 C°/km - Rădulescu et al., 1981) support the existence of some high temperature rocks in the underground, whose density may decrease, and/or thermal convective phenomena along deeper seated faults.

General comments

The hypothesis of a magmatic chamber beneath the Ciomadul volcano had been considered by several geologists (e.g. Szakács et al. 2002; Szakács and Seghedi 2013, Szakács et al, 2015). Large-scale seismic tomography (e.g. Popa et al., 2015) and MT studies (Harangi et al., 2015) seem to confirm the existence of a high-temperature anomaly that could explain the low seismic velocities and high electrical conductivity beneath Ciomadul volcano, but is located significantly deeper (5 – 20 km). Still, the regional scale of the above-mentioned research and their low resolution make difficult an appropriate comparison with data inferred from gravity inversion.

The density anomaly located beneath the Ciomadul volcano seem to be more likely due to the presence of a large volume of low density hot andesitic rocks, similar to those encountered by drillings near Tusnad Bai at about 500 m in depth, where dykes reaching near the surface might explain the presence of local geomagnetic anomalies. The unusually low density of these rocks, never encountered in outcrops, might be due to their high temperature. Vertical asymmetry of the anomalous zone (Fig. 4.3.3.2-4.3.3.5), with higher gradients in the upper side, suggest a faster cooling in the upper part and slower at the bottom, in agreement with the model proposed here.